HAL open science

On the control of dispersion interactions between biological membranes and protein coated biointerfaces

Robert Blackwell, Arnaud Hemmerle, Andreas Baer, Matthias Späth, Wolfgang Peukert, Drew Parsons, Kheya Sengupta, Ana-Sunčana Smith

To cite this version:

Robert Blackwell, Arnaud Hemmerle, Andreas Baer, Matthias Späth, Wolfgang Peukert, et al.. On the control of dispersion interactions between biological membranes and protein coated biointerfaces. Journal of Colloid and Interface Science, 2021, 598, pp.464-473. 10.1016/j.jcis.2021.02.078 . hal-03856763

HAL Id: hal-03856763

https://hal.science/hal-03856763v1

Submitted on 9 May 2023

HAL is a multi-disciplinary open access archive for the deposit and dissemination of scientific research documents, whether they are published or not. The documents may come from teaching and research institutions in France or abroad, or from public or private research centers.

L'archive ouverte pluridisciplinaire **HAL**, est destinée au dépôt et à la diffusion de documents scientifiques de niveau recherche, publiés ou non, émanant des établissements d'enseignement et de recherche français ou étrangers, des laboratoires publics ou privés.

Distributed under a Creative Commons Attribution - NonCommercial 4.0 International License

Version of Record: https://www.sciencedirect.com/science/article/pii/S0021979721002241
Manuscript_0e809b13cbe98e2801820a9584744ece

On the Control of Dispersion Interactions Between Biological Membranes and Protein Coated Biointerfaces

Robert Blackwell[a], Arnaud Hemmerle[b,1], Andreas Baer[a], Matthias Späth[a], Wolfgang Peukert[c], Drew Parsons[d,2], Kheya Sengupta[b,*,3] and Ana-Sunčana Smith[a,e,**,4]

[a] *PULS Group, Department of Physics and Interdisciplinary Center for Nanostructured Films, Friedrich-Alexander-Universität Erlangen-Nürnberg, IZNF, Cauerstrasse 3, 91058 Erlangen, Germany*

[b] *Aix-Marseille Université, Centre Interdisciplinaire de Nanosciences de Marseille, CNRS, UMR 7325, Campus de Luminy, 13288 Marseille cedex 9, France*

[c] *Institute of Particle Technology, Interdisciplinary Center for Functional Particle Systems, Friedrich-Alexander-Universität Erlangen-Nürnberg, Haberstrasse 9a, 91058 Erlangen, Germany*

[d] *Chemistry and Physics, College of Science Health Engineering and Education, Murdoch University, Murdoch 6150, WA, Australia*

[e] *Division of Physical Chemistry, Ruđer Bošković Institute, Bijenička cesta 54, 10000 Zagreb, Croatia*

ARTICLE INFO

Keywords:
Biointerfaces
Dispersion forces
Lifshitz theory
Van der Waals interactions
Reflection interference contrast microscopy (RICM)

Abstract

Hypothesis: Interaction of cellular membranes with biointerfaces is of vital importance for a number of medical devices and implants. Adhesiveness of these surfaces and cells is often regulated by depositing a layer of bovine serum albumin (BSA) or other protein coatings. However, anomalously large separations between phospholipid membranes and the biointerfaces in various conditions and buffers have been observed, which could not be understood using available theoretical arguments.

Methods: Using the Lifshitz theory, we here evaluate the distance-dependent Hamaker coefficient describing the dispersion interaction between a biointerface and a membrane to understand the relative positioning of two surfaces. Our theoretical modeling is supported by experiments where the biointerface is represented by a glass substrate with deposited BSA and protein layers. These biointerfaces are allowed to interact with giant unilamellar vesicles decorated with polyethylene glycol (PEG) using PEG lipids to mimic cellular membranes and their pericellular coat.

Results: We demonstrate that careful treatment of the van der Waals interactions is critical for explaining the lack of adhesiveness of the membranes with protein-decorated biointerfaces. We show that BSA alone indeed passivates the glass, but depositing an additional protein layer on the surface BSA, or producing multiple layers of proteins and BSA results in repulsive dispersion forces responsible for 100 nm large equilibrium separations between the two surfaces.

Abbreviations:
PEG: polyethylene glycol
BSA: bovine serum albumin
RICM: reflection interference contrast microscopy
GUV: giant unilamellar vesicle
SOPC: 1-stearoyl-2-oleoyl-sn-glycero-3-phosphocholine
DOPE-PEG: 1,2-dioleoyl-sn-glycero-3-phosphoethanolamine-N-(methoxy(polyethyleneglycol))
PBS: phosphate buffered saline
ITO: indium tin oxide
CM: Clausius-Mossotti
PLL: polylysine

Symbols:
V_{vdW}: van der Waals potential
A_{H}: Hamaker *function*
h: membrane-substrate separation
d: coating thickness
n: coating surface number density
κ: reciprocal of Debye screening length
ϵ: dielectric function
ξ: frequency
ρ: number density
α: molecular polarizability
ϕ: volume fraction
δ: dielectric increment

1. Introduction

The interactions of biological materials have been actively studied for the better part of a century. Much of the work on these biomaterials has been at the molecular level, where protein-protein and protein-self interactions are the dominant focus. Recent interests in drug delivery, biocompatible implants, directed self-assembly, and colloidal materials necessitate the understanding not only of the molecular level properties of biological materials, but also the semi-bulk interfacial properties of these materials [1]. For example, the collective interactions between layers of material can

*Corresponding author
**Principal corresponding author

rblackwell@flatironinstitute.org (R. Blackwell); arnaud.hemmerle@synchrotron-soleil.fr (A. Hemmerle); andreas.baer@fau.de (A. Baer); matthias91spaeth@gmail.com (M. Späth); wolfgang.peukert@fau.de (W. Peukert); D.Parsons@murdoch.edu.au (D. Parsons); sengupta@cinam.univ-mrs.fr (K. Sengupta); smith@physik.fau.de, asmith@irb.hr (A. Smith)

ORCID(s):

[1] Present address: Synchrotron SOLEIL, Saint Aubin, LOrme des Merisiers, BP48, 91192 Gif-sur-Yvette, France

[2] Present address: Department of Chemical and Geological Sciences, University of Cagliari, Cittadella Universitaria, 09042 Monserrato, CA, Italy

[3] Phone: +33(0)6 60 30 28 62; Fax: +33(0)4 91 41 89 16

[4] Phone: +49 9131 85–70565; Fax: +49 9131 85–70518

© 2021 published by Elsevier. This manuscript is made available under the CC BY NC user license
https://creativecommons.org/licenses/by-nc/4.0/

substantially differ from that of single molecule interactions. These interactions instead lie far beyond the simple pair summation, with the interaction sometimes having counter-intuitive effects such as repulsive van der Waals forces [2]. It is therefore of critical importance that interactions of simple biointerfaces be fully described in order to understand the behavior of the increasingly complex studies on *in vitro* membrane interactions as well as the interactions of *in vivo* biological interfaces [3].

Experimentally, interfacial interactions can be difficult to measure due to the small, typically nanometer, length scales as well as the effects of the immersing solutions on the interactions. Still, several techniques exist to measure interactions between biointerfaces such as the surface force apparatus [4, 5], the colloidal probe technique in atomic force microscopy [6–8], and the total internal reflection fluorescence microscopy [9].

In the context of biological membranes, a particularly suitable technique for studying interface interactions is reflection interference contrast microscopy (RICM) [10–13]. RICM is a label-free microinterferometric technique giving access to the distance between a membrane and a substrate with a $\approx$ 4 nm resolution. A host of experiments have utilized the RICM to probe both the interaction between substrates, coated with protein layers, and membranes of cells or deflated giant unilamellar vesicles (GUVs) [10, 13–20]. When close to the substrate, the vesicle undergoes deformations with constrained volume and area. The vesicle eventually adopts a shape that balances the elastic energy and the effective adhesion strength associated with the depth of the minimum of the non-specific potential [21, 22].

It is widely accepted that the strength and the position of this non-specific minimum results from balancing the membrane-substrate van der Waals and the Coulomb potential with the repulsive Helfrich potential [23–26]. The latter emerges from the suppression of membrane fluctuations, which are dependent on the membrane tension and bending stiffness [27–29]. A more detailed analysis of vesicle shapes pointed out that gravity may play a role in setting the distance between the membrane and the biointerface [30, 31]. Additional steric effects were associated with the membranes whose surface is decorated with glycan chains and other polymeric tethers [32, 33].

Careful measurements of the position of the minimum of the potential [10, 13, 15, 16, 18, 19, 34], however, show a surprising effect. Despite being performed under numerous different solvent conditions, membrane types, and protein coatings, they all exhibit an anomalously distant separation between the membrane and the surface coating. For example, in experiments on a 1-stearoyl-2-oleoyl-sn-glycero-3-phosphocholine (SOPC) membrane interacting with a bovine serum albumin (BSA) coating on glass, the typical mean membrane-surface separation is approximately 80 to 100 nm, while the minimum observed separation is approximately 30 nm (Table 1). However, the fluctuation amplitude in these measurements, being about 10 nm and not exceeding 20 nm, is indicative of the presence of a long range repulsion other than the Helfrich one [34], the latter being characterized by the length scale of the fluctuation amplitude.

In this work, we attempt to understand this positioning of the membrane at the anomalously large separations from the biocompatible supports. Since there are a number of interactions which could drive the observed behavior in the experimental systems and to further motivate this work, we outline the non-specific interactions and ascertain their relative contributions by both basic analysis and a number of experiments. We focus on the effects of a glass substrate with a coating of BSA and proteins on its surface. The free membrane is then modeled as an SOPC layer immersed in aqueous solutions above this surface, since all the measurements are performed with SOPC-based GUVs using the methods outlined in prior works [10, 15, 16, 18, 19, 34, 35]. We perform an in depth analysis of the relevant parameter space within the theoretical framework to demonstrate the sensitivity of the emergent potential and compare to experiments when possible.

We show that the complexity of the membrane and the solid biointerface produces a highly asymmetric system, for which the Hamaker coefficient becomes significantly more complex than in simple symmetric systems traditionally studied. More specifically, we find that the thickness of BSA on the glass surface drastically changes the strength of the membrane-substrate attraction compared to the pure glass system. Thus, a repulsive barrier appears in the potential at membrane-substrate separations of up to approximately 30 nm, which qualitatively agrees with our experiments. Adding additional protein layers may render the van der Waals potential purely repulsive. This leads to the conclusion that the van der Waals forces are a necessary contributor to explain the observed unusually large separations between the membrane and the biointerface.

2. Experimental methods

2.1. Materials

Polylysine(20)-g(3.5)-polyethyleneglycol(5) (PLL-PEG) and Neutravidin were purchased from SUSOS, Switzerland and Invitrogen, Eugene, OR, USA, respectively. DOPE-PEG-2000 (1,2-dioleoyl-sn-glycero-3-phosphoethanolamine-N-(methoxy(polyethyleneglycol)-2000)), DOPE-cap-biotin (1,2-dioleoyl-sn-glycero-3-phosphoethanolamine-N-(cap biotinyl)) and SOPC (1-stearoyl-2-oleoyl-sn-glycero-3-phosphocholine) were purchased from Avanti Polar Lipids (Alabaster, AL, USA) and used without further purification (purity >99 %). Bovine serum albumin (BSA, purity >98 %) and biotinylated BSA (BSA-biotin, purity >80 %) were both purchased from Sigma (Saint Louis, MO, USA) and used after filtering with a 0.2 µm syringe filter.

Thickness-corrected glass coverslips ($d = 170 \pm 10$ µm, Assistent, Karl Hecht KG, Sondheim, Germany), were cleaned by the following detergent treatment: ultrasonication in 10 % Hellmanex solution (Hellma, Müllheim, Germany) for 30 min, flushing thoroughly with ultrapure water from a water purification system (Milli-Q, Millipore, San Francisco, CA, USA)

Table 1
Summary of measured average membrane positioning in experiments on sedimented GUVs.

Mean distance	Membrane	Buffer	Substrate	Reference
30 to 50 nm	DEPC[a] + PEG	HEPES[b]	fat-free milk	[10]
90 to 120 nm	DMPC[c] + PEG	HEPES	fat-free milk+E-selectin	[15]
60 to 80 nm	SOPC + PEG	PBS	BSA	[16, 18]
90 nm	SOPC + PEG	PBS	BSA+Neutravidin	[19]

[a] DEPC - 1,2-dielaidoyl-sn-glycerol-3-phosphocholine
[b] HEPES - 2-(4-(2-Hydroxyethyl)-1-piperazinyl)-ethansulfonacid
[c] DMPC - 1,2-dimyristoyl-sn-glycero-3-phosphocholine

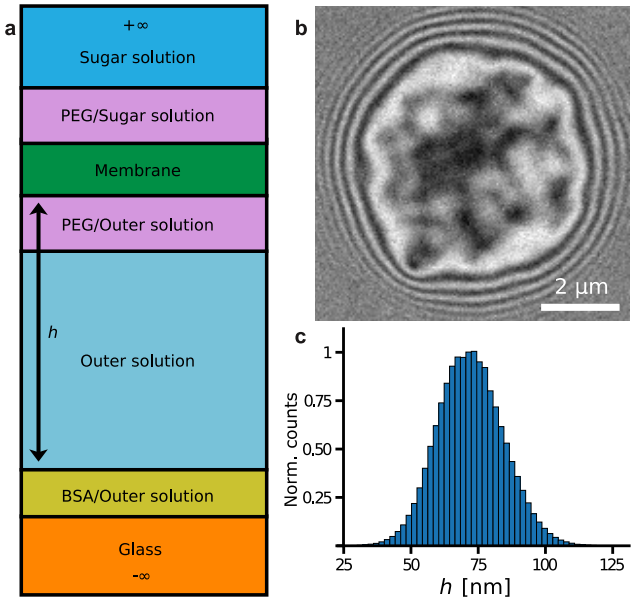

Figure 1: Overview of a system based on a biointerface with a BSA layer. **a**. Schematic of the experimental system used in the van der Waals potential calculation. The reported height is the average over seven vesicles. **b**. Sample RICM image of a DOPE-PEG vesicle in a glucose solution near the surface in the system from panel *a*. **c**. Peak-normalized histogram of height measurements over a full time series and fixed collection area in a single vesicle experiment. The data corresponds to vesicle 5 of the experiment with PBS as outer solution.

and again ultrasonication (2 × 30 min) in 10 % Hellmanex solution, followed by 3 times ultrasonication in ultrapure water for 30 min.

Glucose (purity >99 %), sucrose (purity >99.5 %), and phosphate buffered saline (PBS) were purchased from Sigma in powder form, prepared at the desired concentrations in pure water, and stored at 4 °C for maximum two weeks. The concentrations of the solutes in the 1 × PBS solution were 140 mM NaCl, 3 mM KCl, 10 mM Na_2HPO_4 and 2 mM KH_2PO_4, with a total osmolarity of 300 mOsm. L^{-1}. A solution of 0.5 × PBS was also used, with its osmolarity adjusted by glucose addition to reach 300 mOsm. L^{-1}. All osmolarities were measured before and after each experiment with a cryoscopic osmometer (Osmomat 030, Gonotec GmbH, Berlin).

2.2. GUV and substrate information

GUVs consisting of SOPC with 2 mol % DOPE-PEG-2000 were prepared by the electroswelling method [36], and 2 mol % DOPE-cap-biotin were added to the lipid mixture for the BSA-Neutravidin-BSA experiment. Briefly, 10 mL of a solution of lipids dissolved in chloroform (purity >99.9 %) at 2 mg mL^{-1} was spread on a glass slide coated with indium tin oxide (ITO), and placed in a desiccator under vacuum overnight. The ITO glass slide with the lipid film on it and a second ITO glass slide were mounted on each side of a ≈ 4 mm thick Teflon spacer. The chamber was filled with a 230 mOsm. L^{-1} sucrose solution resulting in the interior of the GUV, later referred to as inner solution. An alternating voltage of 2.2 V at 10 Hz was applied for 4 h, yielding GUVs of about 40 µm average diameter. The vesicle solution was used immediately after production, or stored for maximum 48 h in a fridge at 4 °C.

During an experiment, 20 µL of the vesicle solution was added into the observation chamber filled with 600 mL of the outer solution. Depending on the specific experiment, the latter consists of PBS and/or glucose dissolved in water with its osmolarity adjusted to 300 mOsm. L^{-1}. The observation chamber was covered with a glass slide during the whole experiment to avoid osmolarity changes due to evaporation. The refractive index of each solution was measured with an Abbe refractometer (AR 4D, Krüss GmbH, Hamburg, Germany), taking into account the dependence of the refractive index with the wavelength (cf. SI-Table I for values).

The glass slides were passivated during one hour directly before the experiments with 10 mg mL^{-1} BSA. Excess molecules not bound to the slide were removed by exchanging the buffer against the outer solution in a series of ten washing steps. In the PLL-PEG experiment, 150 µL of PLL-PEG were deposited on the glass slide at a concentration of 1 mg mL^{-1}. Excess molecules not bound to the slide were removed after 1 h in a similar way as with BSA. In the BSA-Neutravidin-BSA experiment, the deposition of the first layer of BSA-biotin was followed by a one hour incubation in 20 µg mL^{-1} Neutravidin dissolved in PBS. Excess Neutravidin was removed by 10 washing steps and finally the second layer of BSA was formed by the incubation of 500 µg mL^{-1} BSA-biotin for one hour.

2.3. Image acquisition and data analysis

RICM images were acquired with an inverted microscope (Axio Observer A1, Zeiss, Jena, Germany) equipped with crossed polarizers and a 63 × Antiflex Plan-Neofluar oil objective with a numerical aperture of 1.25 and a built-in $\lambda/4$ plate. The green line of a metal halide lamp (X-Cite, Exfo, Quebec, Canada) was selected with an interference filter with 546 ± 10 nm. The numerical aperture of illumination was set to approximately 0.5. To achieve maximum contrast, the antiflex technique was applied [37]. Image sequences of vesicles were recorded with an Andor iXon camera (Andor, Belfast, Ireland) and an exposure time of 200 ms. The raw experimental data, and the analysis scripts are accessible as Mendeley Data [dataset][38].

Based on previous work [16, 18, 34, 39] as well as an analysis of data subsets, we find that already 100 frames provide converged information on the average height of a vesicle. Consequently, in our data analysis between 100 and 1500 frames were used, leading to an uncertainty of about 4 nm, as estimated for a fluctuating membrane [12, 34]. This reported uncertainty is not that of the membrane fluctuation amplitude but the experimental error that arises mainly from the shot noise of the camera. The shot noise of the camera can be deconvolved from the true signal [34], in which case the variations in $h(x,t)$ are a direct consequence of the membrane thermal fluctuations. A typical snapshot and from the simulation and a height distribution emerging from the snapshot is shown in Fig. 1b,c.

The contrast of an RICM image results from the interference between the light rays reflected at the different interfaces in a sample, and the membrane-substrate separation $h(x,t)$ can be calculated from the intensity at each pixel x and each frame t of the RICM image [12, 40]. The recorded image at time t is in the form of a matrix of intensities $I(x,t)$ and is converted to a matrix or map of corresponding heights $h(x,t)$ of the vesicle membrane above the substrate. To perform the conversion from intensity to height, first the theoretical relation between I and the corresponding h, defined as the distance from the top of the BSA layer to the bottom of the membrane, is obtained using the Fresnel formalism (see review [12] for details). Thereby, each protein, lipid or buffer (solution) layer is treated as a slab with a smooth interface and having a given thickness and refractive index (SI-Table I).

The first and last layer are set to be the glass substrate and the vesicle inner solution with infinite thickness, respectively. The refractive index of the glass slide is specified by the supplier (Assistent, Karl Hecht KG, Sondheim, Germany), while for the inner and outer buffers, the refractive indices are measured with an Abbe refractometer (AR 4D, Krüss GmbH, Hamburg, Germany).

The thickness of the lipid layer was fixed at 4 nm [12], while the corresponding refractive indices are taken from prior work [16, 41]. In the height reconstruction, the PEG layer can be ignored, as it has a low density of only 2 mol % of lipids and is thus optically transparent.

The morphology of each BSA, Neutravidin or PLL-PEG layer (in terms of homogeneity and roughness) has been controlled using RICM microscopy prior to vesicle injection. Any microscopic or macroscopic defect such as holes or aggregates in the layers would lead to a variation of intensity contrast. Based on previous measurements [34], the thicknesses of the BSA, PLL-PEG and Neutravidin layers were fixed to 10, 3 and 4 nm respectively (see section 4.3). Moreover, prior measurements with AFM showed that equivalent protocols give protein layers where the roughness is of the order of 1 to 2 nm [42]. In the height calculation, the refractive indices of the proteins are taken from the literature [43]. Finally, we have carefully checked that small variations of thickness or refractive index of these layers lead to minor changes in the measured height, within the given error bars of ± 4 nm.

Using these values for the thickness and refractive indices of the respective layers (as summarized in SI-Table I), the functional form of $h(I)$ with respect to the intensity I is written [12, 40]. Normalizing both the theoretical and the experimental $h(I)$, using the background intensity as the normalizing factor, allows us to then effectively read off the value of h that corresponds to the given $I(x)$ in a given pixel x. Treating all the time frames in this way, a distribution of separations $h(x,t)$ is obtained for each vesicle independently (Fig. 1c). Finally the the average height $\langle h \rangle$ is calculated as the mean over all vesicles. The reported standard deviation arises from the variation in the sample.

3. Dominant effectively short-range surface potentials

3.1. Hydration forces

There are three major non-specific interactions between membranes and other surfaces that typically control membrane behavior: hydration, screened coulomb, and van der Waals interactions. We briefly outline them here.

Hydration forces are driven by water molecules near the hydrophilic membrane surface, which attracts nearby water molecules. Removing these water molecules to generate membrane-surface contact requires considerable work, which in turn results in a strong membrane-surface repulsion at separations on the order of a nm [44–47]. While hydration forces certainly play a role at short ranges, they are negligible at the membrane-substrate separation distances typically observed in experiment (30+ nm) [10, 13, 15, 16, 18, 19, 48].

3.2. Screened Coulomb interactions

Screened Coulomb interactions arise from surface charges that are exposed as ions dissociate from their respective interfaces. These surface charges maintain a counter-ion cloud nearby which "screens" the direct Coulomb interaction, where the size and screening strength of the cloud is determined by both the availability of ions in the solution and the temperature. While the specifics of calculating the screened Coulomb interaction for these material configurations can be complicated, the basic range of the interaction is predominantly set by the concentration of ions in the

Table 2
Summary of experiments on GUVs with varying outer solution conditions. The distance distribution mode was measured across six to seven different vesicles for each experimental condition and subsequently averaged. The error provided is the standard deviation over the set of vesicles and the full data series are given in SI-Table II.

NaCl [mM]	glucose [mM]	κ^{-1} [nm]	pH [-]	$\langle h \rangle$ [nm]
0	300	>200	5.3	77 ± 3
70	140	1.1	7.4	90 ± 15
140	0	0.8	7.4	91 ± 14

solution. At the high ionic concentrations ($\approx$ 140 mM) in the experiments, following DLVO theory, the interactions are expected to be on the order of a few nanometers due to the small Debye length $\kappa^{-1} \approx 0.8$ nm [46, 49]. Even at smaller ionic concentration, the range of Coulomb interaction should not exceed a few nanometers.

To test if the screened Coulomb interactions are, despite the prior estimation, a driver for the anomalous repulsion, we performed a series of experiments varying the ionic strength of the outer solution (PBS concentration), while fixing the osmolarity of the outer solution by adding glucose (Table 2). Our current procedure allows us to either have large screening lengths or completely screened electrostatic interactions due to the particular dependence of the Debye length on the inverse of the square root of the concentration. Hence, intermediate screening lengths would require excellent control of low salt concentrations. Notably however, the majority of applications of adherent membrane experiments takes places in the two limiting cases.

With no PBS, the pH of the outer solution drops to approximately that of BSA's isoelectric point of $\approx$ 5 [50, 51], because of dissolution of CO_2 into water [52]. Consequently, the charge on the BSA surface is close to zero, removing a source of the screened Coulomb interaction. Interestingly, even with the lack of charge and reduced screening, there is still clearly a strong repulsion between the substrate and the membrane, which resides at 77 ± 3 nm.

Increasing the concentration of ions indeed slightly increases the membrane-biointerface separation to 90 ± 15 nm. However, this effect is more likely related to changes in the dielectric properties of the solution and the resulting dispersion interactions, as will be shown in the following.

From this series of experiments, it is clear that the screened Coulomb interaction is not directly driving the repulsion in the present systems, and that another mechanism is likely at play. Due to the short-range nature of the screened Coulomb interaction at the experimental ionic concentrations and the weak response of the membrane to ionic concentration shown in our experiments, we focus primarily on the van der Waals interactions as the cause for the large separations.

4. Van der Waals interactions

Van der Waals forces arise from any dipole-dipole interaction (permanent or induced) between two objects. While the van der Waals potential between point particles typically discussed varies steeply with distance (h^{-6}), the potential decays significantly more slowly between two semi-infinite parallel plates, with a leading order of h^{-2}, where h is the membrane-biointerface separation [53]. In this case, the potential is therefore

$$V_{\mathrm{vdW}}(h) = -\frac{A_{\mathrm{H}}}{12\pi h^2}, \tag{1}$$

where A_{H} is the Hamaker coefficient, which depends directly on the bulk dielectric properties of the components in the system of interest. While the Hamaker coefficient is specific to the materials and their configuration being examined, it is typically calculated to be on the order of $k_{\mathrm{B}}T$ (k_{B} being the Boltzmann constant and T temperature) for biological membrane based systems by utilizing Lifshitz theory [46, 54]. However, while often neglected, the Hamaker coefficient also has a separation dependence, altering the simple h^{-2} decay and in some cases considerably changing the qualitative behavior of the system in question [55, 56]. For this reason, we hereafter refer to $A_{\mathrm{H}}(h)$ as the *Hamaker function*.

4.1. Extended Lifshitz theory for calculating the Hamaker function

The Hamaker function, and therefore the van der Waals potential, is determined solely by the dielectric properties and geometry of the system, which we address using Lifshitz theory with code developed for prior work [57–60]. Specifically, to calculate the Hamaker function for the appropriate experimental setups (Fig. 1a), we use the extension of Lifshitz theory to multiple layers from Parsegian and Ninham [61]. This approach generates a dispersion interaction potential which has subtracted the interfacial energy of each surface [62].

Fundamentally, Lifshitz theory is a summation of the free energy contribution of electromagnetic field fluctuations within a given material configuration. Electromagnetic field fluctuations are decomposed into oscillatory modes extending through the analyzed body, restricted by the material properties and dimensions of the body [53], with each mode having an associated electromagnetic free energy. The total free energy for a given material configuration is completely determined by the differences between each material's dielectric function evaluated at the discrete frequencies ξ_n. At room temperature the first non-zero frequency is infrared and typically the main frequencies contributing to the van der Waals interaction are below the soft X-ray region [63]. Therefore, accurate calculation of the interaction requires a nearly complete dielectric function for each material within the system.

4.1.1. The dielectric functions of mixtures

While there is a relative wealth of data on the dielectric functions of pure materials, those of mixtures are less well characterized. We therefore make heavy use of the Clausius-Mossotti (CM) mixture relation in our calculations for dielectric functions at non-zero frequencies. This relation comes in two equivalent forms, both given here for convenience. The CM relation with known polarizability is

$$\epsilon(\xi) = 1 + \frac{4\pi \sum_i \rho_i \alpha_i(\xi)}{1 - \frac{4\pi}{3} \sum_i \rho_i \alpha_i(\xi)}, \tag{2}$$

where ρ_i is the number density of each component within the layer, α_i is the molecular polarizability of the component, and ξ is the frequency. The CM relation for dielectric mixtures is

$$\frac{\epsilon(\xi) - 1}{\epsilon(\xi) + 2} = \sum_i \phi_i \frac{\epsilon_i(\xi) - 1}{\epsilon_i(\xi) + 2}, \tag{3}$$

where ϕ_i is the volume fraction of each component in the layer [64].

We treat the dielectric constant $\epsilon(0)$ separately by using experimental measurements directly when available. These measurements are either already completed for the mixture (as in the case of the lipid headgroup), or are provided as a parameter in our model. For aqueous mixtures, the dielectric constant is that of water plus a term that is linearly dependent on the concentration of the solute. The coefficient defining this change is known as the dielectric increment/decrement, depending on the sign of the change, and is defined as

$$\delta_{\text{solute}} = \lim_{c \to 0} \frac{\epsilon_{\text{solution}}(0) - \epsilon_{\text{solvent}}(0)}{c} \tag{4}$$

where c is the concentration of the solute in the mixture [65]. The dielectric constant of an aqueous mixture is then approximately $\epsilon_w(0) + \delta c$. When no decrement is provided, we use a linear combination of the two materials

$$\epsilon_{\text{solution}}(0) = \sum_i \epsilon_i(0)\phi_i, \tag{5}$$

where $\epsilon_i(0)$ is the dielectric constant of each component, as is appropriate for aqueous solutions [56].

4.1.2. Parametrization of the system

The relatively large number of parameters requires a careful analysis of available models for each material in the layered structure. To address this issue we perform a sensitivity study for each sub-layer about a central consistent "best guess" parameter set for the whole system (see SI for details). Specifically, the semi-infinite glass support is modeled using the dielectric function from Masuda et al. [66], yet other models [67, 68] provide nearly indistinguishable results. Describing water is more delicate, with the available approaches by Parsegian and Weiss [69], Tavares et al. [70], Dagastine et al. [63] and Masuda et al. [66], providing somewhat different results (see SI section VI A). However, from all models only the data from Dagastine et al. [63] is purely experimental and is hence directly used in this work. Other approaches are rather a model fit [66, 69, 70], as is the more recent version [71], which fits the results of Dagastine et al. [63] very well.

PBS is approximated to be an aqueous solution with 140 mM NaCl, neglecting the low concentration contributions from the phosphates and potassium. Furthermore, the CM relation was used to calculate the permittivity of the solution at non-zero frequencies. Polarizabilities for the non-zero frequency component are taken from Parsons and Ninham [72] while for the zero frequency permittivity, we use the dielectric decrement of $-11\,\text{M}^{-1}$ NaCl [65, 73]. The sugar solution is sucrose in water at concentrations of approximately 230 mM as typically used in experiments [10, 13, 15, 16, 18, 19, 48]. The details of the dielectric functions can be seen in SI sections VI B and VI C.

The membrane (SOPC) is modeled as a three-layer system of two headgroup layers with a tail layer between them. Due to their carbohydrate nature and equivalent length, the tails are represented by hexadecane with the polarizability data taken from Masuda et al. [66]. The headgroup is modeled as a mixture of choline, dihydrogen phosphate, and glycerol using the CM mixture relation (equation 2). The polarizability of each segment was calculated using Density Functional Theory (cf. SI section IV A 2). The value of the headgroup's dielectric constant is tightly constrained by experiments to $\epsilon_{\text{head}}(0) \approx 25$ to 45 [74–80], and its choice basically does not affect the van der Waals potential (SI-Fig. 1).

The common carbohydrate-rich layer present in mimetic and cell membranes is constructed from the PEG, with molecular weight 2 kDa (PEG-2000) bound to a small fraction of the lipid headgroups at the density of roughly $3.2 \times 10^{-2}\,\text{nm}^{-2}$ at 2 mol % [10, 81–83]. We model the PEG layer as a mixture of PEG with the appropriate surrounding solution (cf. SI section V). To account for the unknown distribution of PEG we first assume a uniform layer with a thickness of ≈ 3.4 nm, PEG-2000's Flory radius. In the second model, we use a simple parabolic model for the volume fraction of PEG as a function of distance from the membrane [83]. The effects of PEG appear on the short range van der Waals interactions only, particularly at thicker protein layers on the biointerface (SI-Fig. 2).

For the BSA, ideally, we would use the dielectric function measured in a hydrated state [84], however, this data is relatively absent in the literature besides the zero frequency limit by Eden et al. [84]. We therefore use the spectroscopic properties of *dry* BSA in the appropriate range ($\approx 5 \times 10^{14}$ to 2×10^{16} Hz) from Inagaki et al. [85], which was fit to a damped harmonic oscillator model to get the appropriate dielectric function for dry BSA [86]. Wet conditions are then obtained using mixing rules with appropriate solvent. At zero frequency, we calculate the polarizability using the dielectric increment of BSA (equation 4) with reported values of $\delta_{\text{BSA}} = 0.1$ to $0.3\,\text{mL}\,\text{mg}^{-1}$, whereby $\delta_{\text{BSA}} = 0.3\,\text{mL}\,\text{mg}^{-1}$ was used as baseline. The full details for the calculation of the dielectric function can be found in

SI section III.

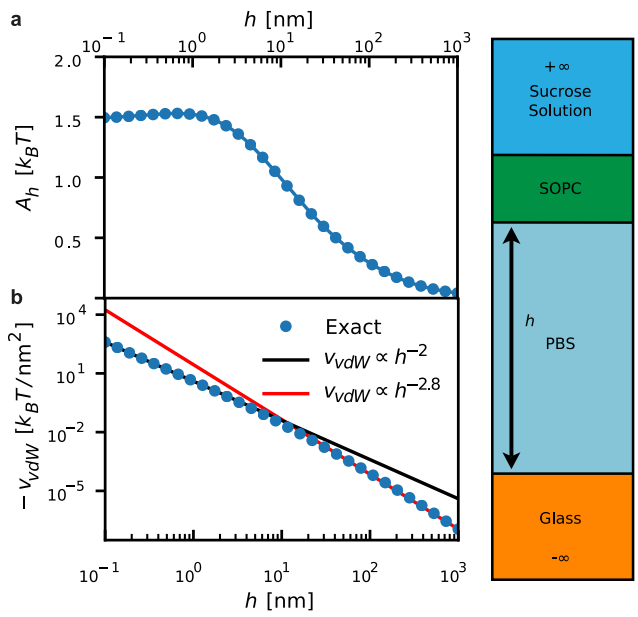

Figure 2: Lifshitz calculations for a simple membrane-glass system as in the right panel. **a**. Hamaker function for the membrane-glass system. **b**. Van der Waals potential for the membrane-glass system. Fits to the short and long range show a transition from a h^{-2} toward a h^{-3} decay in the van der Waals potential.

4.2. Symmetric membrane-biointerface systems

To validate our approach we first analyze a simple, nearly symmetric material configuration. In such systems, at short ranges, the variation in the Hamaker function is typically negligible, but at longer ranges it can decay by orders of magnitude, resulting in a long range van der Waals potential that decays roughly as h^{-3} (Fig. 2) [87]. We find that our calculations for the decay of the Hamaker function are in good agreement with prior calculations on supported bilayer systems, which found a short range limit of the Hamaker function of $\approx 1.3\, k_B T$ and a similar drop in value near 10 nm (Fig. 2a) [52]. For completeness, we note that this separation dependence in the membrane literature is often coded into the approximation

$$V_{\mathrm{vdW}}(h) \approx -\frac{A_{\mathrm{H}}}{12\pi}\left[\frac{1}{h^2} - \frac{2}{(h+D)^2} + \frac{1}{(h+2D)^2}\right], \quad (6)$$

where D is the membrane thickness and the Hamaker function is assumed to be constant [26, 88]. This approximation is reasonable when the interactions are confined to short ranges in symmetric systems [2, 87], but due to the structure of the Hamaker function in more complicated geometries, it can give dramatically different results than a full treatment. In this work, we therefore explicitly calculate the full Hamaker function's separation dependence and test the validity of the assumptions for common configurations of materials.

4.3. Asymmetry introduced by a BSA layer

BSA typically forms a monolayer when deposited onto glass. The thickness and surface density of the BSA layer is incredibly sensitive to the state of the substrate, the pH of the solution during deposition, the concentration of the BSA in solution [51, 89], and even the cleaning procedure may affect the deposition. Therefore, depositing passivating layers on glass must be performed with particular prudence.

BSA is usually approximated as a prolate ellipsoid with a minor axis of 4 nm and major axis of 14 nm [90]. This highly asymmetrical shape then gives rise to two main possible deposition configurations: end-on or side-on. While BSA mostly seems to prefer a side-on deposition (4 nm layer) [51, 89, 91], some conditions of the deposition technique have been shown to alter this behavior such as the pH and BSA concentration during deposition leading to 8 nm BSA layers, suggesting partially overlapping layers [51, 89]. Even when the majority of the BSA is in the side-on configuration, experiments suggest that a fraction of the BSA remains in the end-on configuration, where Bowen et al. [92] found maximum peak-to-valley distances on the BSA layer of $\approx$ 13 nm. Hence the expected thickness of the layer is between 4 and 14 nm.

Due to the sensitivity of the surface density of BSA on the conditions of deposition [51, 89, 91], we first explore the effect of the BSA layer surface density A. For 8 nm thick films, increasing the density results in a small but clear trend of BSA weakening the attractive strength of the van der Waals potential (Fig. 3a). For the end-on configuration of BSA ($d_{\mathrm{BSA}} = 14$ nm), this effect is amplified, leading to a short range ($h = 5$ to 10 nm) repulsion (Fig. 3a inset). While this counter-intuitive behavior is potentially surprising at first, since symmetric systems of interacting materials are guaranteed to be attractive, asymmetric systems are known to be capable of exhibiting repulsive van der Waals forces [93–96].

The effect of the thickness change of the BSA layer is demonstrated directly in Figure 3b, where d_{BSA} is changed systematically, leading to an order of magnitude decrease in the attractive van der Waals energy. This layer size effect would also be amplified considerably by the likely much higher surface density of BSA packed on the surface end-on, as in Fig. 3a inset. This repulsion is primarily driven by the dielectric increment and high relative concentration of protein on the surface, which can lead to the dielectric constant of the layer being significantly higher than that of water.

4.4. Protein layers introduce long-range repulsion

At zero frequency, the dielectric increment for many common proteins can be substantially higher than for BSA, approaching $\delta \approx 1$ mL mg^{-1} [65, 97–99]. The consequence of it can be directly seen when varying only the dielectric increment of the protein coating, where higher increments generically weaken the attractive strength of the van der Waals potential (Fig. 3c). While all potentials are attractive at very short ranges of $\approx$ 1 nm, at intermediate ranges,

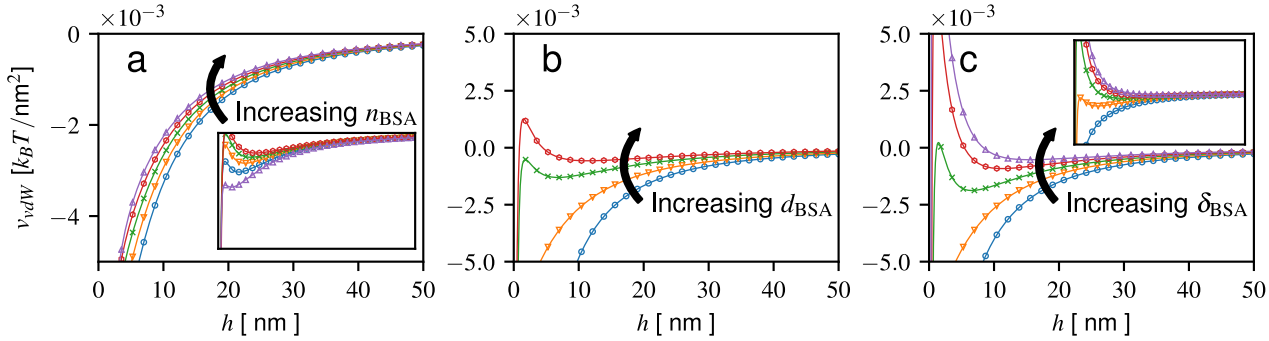

Figure 3: Van der Waals potentials with varying BSA parameters. For panels a and c, main plots are for 8 nm thick BSA layers, while insets are for systems with 14 nm thick BSA layers. **a**. Van der Waals potential versus PEG-BSA separation h for a BSA coating with dielectric increment $\delta_{BSA} = 0.3\,\mathrm{mL\,mg^{-1}}$ and varying surface density $n_{BSA} = 0.008\,15$, $0.012\,25$, 0.0163, $0.020\,375$ and $0.024\,45\,\mathrm{nm^{-2}}$. **b**. Van der Waals potential versus PEG-BSA separation h for a BSA coating of varying thickness $d_{BSA} = 4$, 8, 14 and 20 nm, dielectric increment $\delta_{BSA} = 0.3\,\mathrm{mL\,mg^{-1}}$, and surface density $n_{BSA} = 0.0163\,\mathrm{nm^{-2}}$. **c**. Van der Waals potential versus PEG-BSA separation h for a BSA coating with surface density $n_{BSA} = 0.0163\,\mathrm{nm^{-2}}$, and varying dielectric increment $\delta_{BSA} = 0.1$, 0.3, 0.5, 0.7 and $0.9\,\mathrm{mL\,mg^{-1}}$.

calculations suggest that the potential becomes repulsive for the higher dielectric increments observed in many common proteins, albeit vanishing from below at large distances > 50 nm.

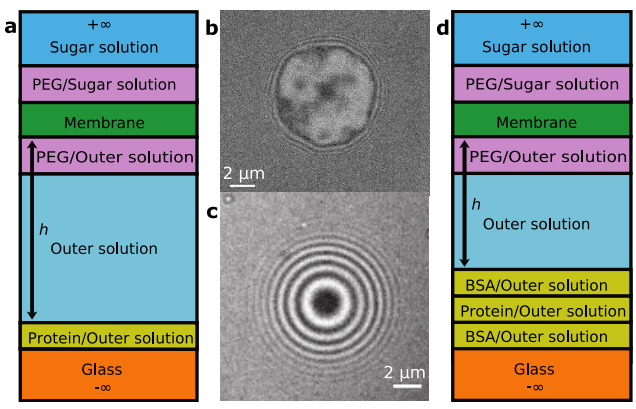

Figure 4: GUVs above different biointerfaces. **a**. The schematics represents the system with a PLL-PEG protein layer. The reported height is a result of averaging over seven GUVs. **b**. Image of a typical contact zone of a GUV in a system as in panel *a*. **c**. Image of a typical GUV in a system as in panel *d* demonstrating the lack of contact. **d**. The schematics represents a system with a layered structure by depositing BSA-Neutravidin-BSA on the glass substrate.

The weakening of the attraction by using a protein layer with a higher dielectric increment is confirmed experimentally by depositing PLL-PEG (Fig. 4a). Indeed we observe that the average separation between the biointerface and the GUV surface increases from 77 ± 4 nm measured with BSA to 93 ± 4 nm (Fig. 4b). This result is consistent with the previously reported data in Table 1 which involves biointerfaces with various protein deposits either directly on glass or on an underlying layer of BSA.

Following this, we performed an experiment by creating a BSA-Neutravidin-BSA multilayer (Fig. 4d) as described in section 2.2. As expected, no GUVs were able to form a contact zone on the protein substrate (Fig. 4c), instead remaining approximately spherical above the surface. This suggests that the attractive component of the van der Waals potential is negligible for thicker protein layers (Fig. 4), in quantitative agreement with the trends predicted in Fig. 3.

5. Discussion

We constructed a series of functional biointerfaces in which we varied the protein layers in thickness and composition, as well as the ionic strength of the surrounding buffers. In agreement with previous studies, we find that abundantly depositing BSA makes the overall strength of the membrane-substrate potential weak. This is evident from the strong fluctuations of the membrane (average amplitude of 10 to 20 nm) around its mean position between 60 and 70 nm away from the top of the BSA surface [10, 13, 15, 16, 18, 19, 48]. Depositing proteins with higher dielectric increment results in GUVs spreading at anomalously high separations of the order of 100 nm, with the same fluctuation amplitude. Producing multilayered BSA-protein composites produces a simply repulsive potential for the GUV, which consequently is not spreading.

Since the overall potential between the membrane and the functionalized biointerface is at first order approximation a superposition of various contributions, we analyze each possible source of this behaviour. First, the positioning of the membrane takes place under the influence of gravity. The latter induces sedimentation and is a source of a very weak attraction. The strength of it can be estimated from the density difference between the inner and outer buffers and the size of the vesicle measured independently. For a vesicle with a size of $D = 40\,\mu\mathrm{m}$, a height above the substrate $h = 100$ nm and g the gravitational acceleration

and using a very generous estimate for the density difference of $\Delta\rho = 0.5\rho_0$ with the density of water $\rho_0 = 1\,\mathrm{g\,cm^{-3}}$, this gives $E/A = \Delta\rho Dhg$ as the energy per unit area of $4.7 \times 10^{-6}\, k_\mathrm{B}T/\mathrm{nm}^2$, with $k_\mathrm{B}T = 4.14\,\mathrm{pN\,nm}$. For the vesicle to spread at 100 nm away from the surface, this very weak attraction must be balanced by an equally weak, long-range repulsion. Notably, the significant spread in the vesicle sizes in the sample should give rise to large spread in mean position of the membrane, which indeed seems to be the case.

Typically, steric interactions are considered to be the main systematic source of repulsion in these systems [23–26, 32, 33]. However, the steric repulsion of the PEG layer decays within 5 nm, the BSA may provide at most 15 nm and the steric repulsion of the membrane adds about 10 to 20 nm. Added all together, this would account for separations of 30 to 40 nm separations, as often observed in protein-mediated adhesion. Thus, the separations of 80 to 100 nm cannot be accounted for by the steric repulsion alone and additional long-range interactions are necessary to explain the result.

We tested if Coulomb interactions could be responsible for the unexpected behaviour of the membrane. We therefore studied the two limiting regimes (large Debye length of >200 nm, or to completely screen the electrostatic interaction). Naturally, in some intermediate regime of partial screening, Coulomb interactions could provide additional long range interactions. However, in the current situation, this is not the case. Given that large separations between the membrane and the biointerface persist even in the limits of very weak or fully screened Coulomb forces, van der Waals interactions are considered to be the source of the weak repulsion.

In the detailed calculation of the van der Waals potentials we find that variations in each layer and its material's dielectric function provide a complex behavior of the Hamaker function. We systematically vary all parameters within their experimentally reported range of magnitudes. The effects of this variation on the intensity of disperse forces are summarized in Table 3, where we show the effect of increasing the magnitude of a particular parameter (keeping everything else constant) (see SI sections III to VI for details). We show that the van der Waals attraction has different sensitivity to various parameters, which may affect the potential at short or long range. For example, increasing the PEG volume fraction on the membrane surface strengthens the van der Waals attraction even though this layer also acts as a steric barrier at small separations between the membrane and the biointerface. Similarly, besides screening the Coulomb interactions, increasing the concentration of ions in the outer buffer makes the van der Waals potential more repulsive at long range, consistent with our experimental results (Table 2).

It is, however, the dielectric behavior of proteins that can significantly alter the van der Waals interaction of a membrane with a biointerface. In agreement with our experimental observations, we find that the interaction is weakened by roughly an order of magnitude with the addition of a protein layer to glass, but for thick proteins or those with high dielectric increments long range repulsion can appear in the potential (Fig. 3c) and balance the gravity. Because the contribution of a given layer to the Hamaker function decays $\propto e^{-h/d}$ where d is the layer thickness, the amount of the material deposited on the biointerface is important.

Table 3
Qualitative summary of the response of the van der Waals interaction to material parameters, roughly sorted by the sensitivity.

Parameter (increasing)	Attraction	Strength
Long-range effects		
Protein dielectric increment	weakens	very strong
Protein thickness	weakens	strong
Protein concentration	weakens	intermediate
Inner solution sucrose conc.	strengthens	intermediate
Outer solution ion conc.	weakens	weak
Short-range effects		
Headgroup area	weakens	weak
Headgroup thickness	weakens	weak
PEG volume fraction	strengthens	weak
Headgroup ϵ_0	strengthens	very weak

Many experiments in the literature rely on BSA depositing in ≈ 4 nm layers, but if this layer is smooth, its contributions would only be significant up to ≈ 10 nm. Increasing the thickness of the passivating deposit, by having BSA oriented with the major axis perpendicular to the interface, may first make the system quite sensitive. In this case the Hamaker function at small separations is typically close to zero (inset of Fig. 3c), and small changes in the dielectric function of any of the materials can drive very drastic changes in behavior, often switching between repulsive and attractive behavior as the Hamaker function changes sign. Reliable long range van der Waals forces require a thick slab of material, which are, in our experiments realized by using protein deposits on BSA, even though more substantial effects were obtained by making multilayered structures (Fig. 4). We here caution that a naïve application of a Hamaker constant as in eq. (6) to more complex biointerfaces ignores the structure of the actual Hamaker function. This can give orders of magnitude large errors in the short range van der Waals interaction energy, drastically skewing the results.

6. Conclusions

This manuscript is inspired by the body of work on interactions of GUVs with functional biointerfaces in which spreading of vesicles occurs at such anomalously high membrane-substrate separations that cannot be explained by steric and Coulomb interactions [10, 15, 16, 18, 19]. Interestingly, these separations were not only observed in mimetic systems but also in adherent cells [100]. It also addresses the commonly observed extreme sensitivity of these systems to preparation procedures and even sources and batches of materials used for the functionalization of glass.

We devise a bottom up experimental approach that systematically adds layer by layer of various materials to the biointerface and the mimetic membrane. This allows us to clearly associate the effect with its cause — increasing the asymmetry of the system and the thickness of the deposited layers renders the van der Waals interactions less and less attractive, until they eventually become repulsive. We corroborate the importance of this layering by theoretical calculations, which provide a repulsive van der Waals potential for reasonable parameters. However, we show that this repulsion indeed relies on the layer with a higher dielectric increment (here provided by proteins), which is the key result of the paper. This layering is also associated with a complex Hamaker function which is difficult to predict a priori.

In closing, our combined experimental and theoretical study highlights the importance of dispersion interactions in the control of the adhesiveness of biointerfaces. It also establishes a methodology for tuning the attractiveness of the surface without relying on the ionic conditions. This may be useful in the preparation of many different biointerfaces that are used in contact with living cells. The applicability and the long-term stability of these layered structures is yet to be established and will be subject of future investigations.

CRediT authorship contribution statement

Robert Blackwell: Methodology, Software, Validation, Formal analysis, Investigation, Writing - Original Draft, Writing - Review & Editing, Visualization. **Arnaud Hemmerle:** Methodology, Software, Validation, Investigation, Writing - Review & Editing. **Andreas Baer:** Validation, Investigation, Writing - Original Draft, Writing - Review & Editing, Visualization. **Matthias Späth:** Methodology, Software, Validation, Formal analysis, Investigation, Writing - Review & Editing, Visualization. **Wolfgang Peukert:** Conceptualization, Writing - Review & Editing. **Drew Parsons:** Methodology, Software, Supervision, Writing - Review & Editing. **Kheya Sengupta:** Conceptualization, Methodology, Investigation, Resources, Writing - Review & Editing, Supervision, Project administration, Funding acquisition. **Ana-Sunčana Smith:** Conceptualization, Methodology, Investigation, Resources, Writing - Original Draft, Writing - Review & Editing, Supervision, Project administration, Funding acquisition.

Acknowledgments

RB thanks the Humboldt foundation for support. ASS, AB and KS were funded by the joint German Science Foundation and the French National Research Agency project SM 289/8-1, AOBJ: 652939. AH and KS acknowledge AMIDEX grant AFFINITY. DFP acknowledges the support of resources from the National Computational Infrastructure (NCI Australia), an NCRIS enabled capability supported by the Australian Government.

References

[1] C. M. Niemeyer, Angewandte Chemie International Edition 40 (2001) 4128–4158. doi:10.1002/1521-3773(20011119)40:22<4128::AID-ANIE4128>3.0.CO;2-S.

[2] V. A. Parsegian, Van Der Waals Forces, Cambridge University Press, 2006. doi:10.2277/0521839068.

[3] P. Shende, V. S. Wakade, Journal of Drug Targeting 28 (2020) 456–467. URL: https://doi.org/10.1080/1061186X.2020.1720218. doi:10.1080/1061186X.2020.1720218. arXiv:https://doi.org/10.1080/1061186X.2020.1720218, pMID: 31961758.

[4] J. N. Israelachvili, D. Tabor, Proceedings of the Royal Society of London. A. Mathematical and Physical Sciences 331 (1972) 19–38. doi:10.1098/rspa.1972.0162.

[5] J. N. Israelachvili, G. E. Adams, Nature 262 (1976) 774–776. doi:10.1038/262774a0.

[6] W. A. Ducker, T. J. Senden, R. M. Pashley, Nature 353 (1991) 239–241. doi:10.1038/353239a0.

[7] H.-J. Butt, Biophysical Journal 60 (1991) 1438–1444. doi:10.1016/S0006-3495(91)82180-4.

[8] M. Götzinger, W. Peukert, The Journal of Adhesion 80 (2004) 223–242. URL: https://doi.org/10.1080/00218460490279297. doi:10.1080/00218460490279297. arXiv:https://doi.org/10.1080/00218460490279297.

[9] C. M. Roth, A. M. Lenhoff, Langmuir 11 (1995) 3500–3509.

[10] S. Marx, J. Schilling, E. Sackmann, R. Bruinsma, Physical Review Letters 88 (2002) 138102. doi:10.1103/PhysRevLett.88.138102.

[11] J. Schilling, K. Sengupta, S. Goennenwein, A. R. Bausch, E. Sackmann, Physical Review E 69 (2004) 021901.

[12] L. Limozin, K. Sengupta, ChemPhysChem 10 (2009) 2752–2768. doi:10.1002/cphc.200900601.

[13] C. Monzel, D. Schmidt, U. Seifert, A.-S. Smith, R. Merkel, K. Sengupta, Soft Matter 12 (2016) 4755–4768. doi:10.1039/C6SM00412A.

[14] A.-S. Smith, B. G. Lorz, S. Goennenwein, E. Sackmann, Biophysical Journal 90 (2006) L52–L54. URL: https://doi.org/10.1529/biophysj.105.079426. doi:10.1529/biophysj.105.079426.

[15] B. G. Lorz, A.-S. Smith, C. Gege, E. Sackmann, Langmuir 23 (2007) 12293–12300. doi:10.1021/la701824q.

[16] C. Monzel, S. F. Fenz, R. Merkel, K. Sengupta, ChemPhysChem 10 (2009) 2828–2838. doi:10.1002/cphc.200900645.

[17] A.-S. Smith, S. F. Fenz, K. Sengupta, EPL (Europhysics Letters) 89 (2010) 28003. doi:10.1209/0295-5075/89/28003.

[18] C. Monzel, S. F. Fenz, M. Giesen, R. Merkel, K. Sengupta, Soft Matter 8 (2012) 6128–6138. doi:10.1039/C2SM07458C.

[19] S. F. Fenz, A.-S. Smith, R. Merkel, K. Sengupta, Soft Matter 7 (2011) 952–962. doi:10.1039/C0SM00550A.

[20] T. Bihr, S. Fenz, E. Sackmann, R. Merkel, U. Seifert, K. Sengupta, A.-S. Smith, Biophysical Journal 107 (2014) L33 – L36. URL: http://www.sciencedirect.com/science/article/pii/S0006349514011163. doi:https://doi.org/10.1016/j.bpj.2014.10.033.

[21] U. Seifert, R. Lipowsky, Phys. Rev. A 42 (1990) 4768–4771. URL: https://link.aps.org/doi/10.1103/PhysRevA.42.4768. doi:10.1103/PhysRevA.42.4768.

[22] U. Seifert, Zeitschrift für Physik B Condensed Matter 97 (1995) 299–309. URL: https://doi.org/10.1007/BF01307480.

[23] R. Lipowsky, S. Leibler, Physical Review Letters 56 (1986) 2541–2544. doi:10.1103/PhysRevLett.56.2541.

[24] S. Leibler, R. Lipowsky, Physical Review B 35 (1987) 7004–7009. doi:10.1103/PhysRevB.35.7004.

[25] G. Fragneto, T. Charitat, F. Graner, K. Mecke, L. Perino-Gallice, E. Bellet-Amalric, EPL (Europhysics Letters) 53 (2001) 100. doi:10.1209/epl/i2001-00129-8.

[26] K. R. Mecke, T. Charitat, F. Graner, Langmuir 19 (2003) 2080–2087. doi:10.1021/la026606d.

[27] W. Helfrich, Zeitschrift für Naturforschung C 28 (1973) 693 – 703. URL: https://www.degruyter.com/view/journals/znc/28/11-12/article-p693.xml. doi:https://doi.org/10.1515/znc-1973-11-1209.

[28] U. Seifert, Phys. Rev. Lett. 74 (1995) 5060–5063. URL:

https://link.aps.org/doi/10.1103/PhysRevLett.74.5060. doi:10.1103/PhysRevLett.74.5060.

[29] J. O. Rädler, T. J. Feder, H. H. Strey, E. Sackmann, Phys. Rev. E 51 (1995) 4526–4536. URL: https://link.aps.org/doi/10.1103/PhysRevE.51.4526. doi:10.1103/PhysRevE.51.4526.

[30] M. Kraus, U. Seifert, R. Lipowsky, Europhysics Letters (EPL) 32 (1995) 431–436. URL: https://doi.org/10.1209%2F0295-5075%2F32%2F5%2F009. doi:10.1209/0295-5075/32/5/009.

[31] J. R. Henriksen, J. H. Ipsen, The European Physical Journal E 9 (2002) 365–374. URL: https://doi.org/10.1140/epje/i2002-10091-3.

[32] R. Lipowsky, Colloids and Surfaces A: Physicochemical and Engineering Aspects 128 (1997) 255 – 264. URL: http://www.sciencedirect.com/science/article/pii/S0927775796039064. doi:https://doi.org/10.1016/S0927-7757(96)03906-4, a collection of papers presented at the 11th International Symposium on Suryactants in Solution.

[33] R. Bruinsma, A. Behrisch, E. Sackmann, Physical Review E 61 (2000) 4253–4267. doi:10.1103/PhysRevE.61.4253.

[34] D. Schmidt, C. Monzel, T. Bihr, R. Merkel, U. Seifert, K. Sengupta, A.-S. Smith, Physical Review X 4 (2014) 021023. doi:10.1103/PhysRevX.4.021023.

[35] S. F. Fenz, T. Bihr, D. Schmidt, R. Merkel, U. Seifert, K. Sengupta, A.-S. Smith, Nature Physics 13 (2017) 906–913. URL: https://doi.org/10.1038/nphys4138.

[36] M. I. Angelova, D. S. Dimitrov, Faraday Discussions of the Chemical Society 81 (1986) 303–311. doi:10.1039/DC9868100303.

[37] J. Ploem, Reflection-Contrast Microscopy as a Tool for Investigation of the Attachment of Living Cells to a Glass Surface, Blackwell, Oxford, 1975.

[38] R. Blackwell, A. Hemmerle, A. Baer, M. Späth, W. Peukert, D. Parsons, K. Sengupta, A.-S. Smith, On the control of dispersion interactions between biological membranes and protein coated biointerfaces, Mendeley Data, 2021. doi:10.17632/pb46knndz2.1.

[39] C. Monzel, D. Schmidt, C. Kleusch, D. Kirchenbüchler, U. Seifert, A.-S. Smith, K. Sengupta, R. Merkel, Nature Communications 6 (2015) 8162. URL: https://doi.org/10.1038/ncomms9162.

[40] L. Limozin, K. Sengupta, Biophysical Journal 93 (2007) 3300–3313. doi:10.1529/biophysj.107.105544.

[41] C. S. Chong, K. Colbow, Biochimica et Biophysica Acta (BBA) - Biomembranes 436 (1976) 260–282. doi:10.1016/0005-2736(76)90192-9.

[42] F. Pi, P. Dillard, R. Alameddine, E. Benard, A. Wahl, I. Ozerov, A. Charrier, L. Limozin, K. Sengupta, Nano Letters 15 (2015) 5178–5184. URL: https://doi.org/10.1021/acs.nanolett.5b01400. doi:10.1021/acs.nanolett.5b01400. arXiv:https://doi.org/10.1021/acs.nanolett.5b01400, pMID: 26161675.

[43] K. Spaeth, A. Brecht, G. Gauglitz, Journal of Colloid and Interface Science 196 (1997) 128 – 135. URL: http://www.sciencedirect.com/science/article/pii/S0021979797952000. doi:https://doi.org/10.1006/jcis.1997.5200.

[44] E. Schneck, F. Sedlmeier, R. R. Netz, Proceedings of the National Academy of Sciences 109 (2012) 14405–14409. doi:10.1073/pnas.1205811109.

[45] R. P. Rand, V. A. Parsegian, Biochimica et Biophysica Acta (BBA) - Reviews on Biomembranes 988 (1989) 351–376. doi:10.1016/0304-4157(89)90010-5.

[46] R. Lipowsky, E. Sackmann, et al., Structure and Dynamics of Membranes 1 (1995) 521–602.

[47] S. Marčelja, N. Radić, Chemical Physics Letters 42 (1976) 129–130. doi:10.1016/0009-2614(76)80567-2.

[48] J. Solon, P. Streicher, R. Richter, F. Brochard-Wyart, P. Bassereau, Proceedings of the National Academy of Science 103 (2006) 12382–12387. doi:10.1073/pnas.0601400103.

[49] X. Xing, Physical Review E 83 (2011) 041410. doi:10.1103/PhysRevE.83.041410.

[50] S. Ge, K. Kojio, A. Takahara, T. Kajiyama, Journal of Biomaterials Science, Polymer Edition 9 (1998) 131–150. doi:10.1163/156856298X00479.

[51] T. J. Su, J. R. Lu, R. K. Thomas, Z. F. Cui, The Journal of Physical Chemistry B 103 (1999) 3727–3736. doi:10.1021/jp983580j.

[52] A. Hemmerle, L. Malaquin, T. Charitat, S. Lecuyer, G. Fragneto, J. Daillant, Proceedings of the National Academy of Sciences 109 (2012) 19938–19942. doi:10.1073/pnas.1211669109.

[53] J. N. Israelachvili, Intermolecular and Surface Forces, Academic Press, 2011.

[54] P. Attard, D. J. Mitchell, B. W. Ninham, Biophysical Journal 53 (1988) 457–460.

[55] E. R. Smith, D. J. Mitchell, B. W. Ninham, Journal of Colloid and Interface Science 45 (1973) 55–68. doi:10.1016/0021-9797(73)90242-7.

[56] R. R. Dagastine, M. Bevan, L. R. White, D. C. Prieve, The Journal of Adhesion 80 (2004) 365–394. doi:10.1080/00218460490465696.

[57] D. F. Parsons, M. Boström, P. Lo Nostro, B. W. Ninham, Physical Chemistry Chemical Physics 13 (2011) 12352–12367. doi:10.1039/C1CP20538B.

[58] D. F. Parsons, A. Salis, Current Opinion in Colloid & Interface Science 23 (2016) 41–49. doi:10.1016/j.cocis.2016.05.005.

[59] D. F. Parsons, B. W. Ninham, The Journal of Physical Chemistry A 113 (2009) 1141–1150. doi:10.1021/jp802984b.

[60] D. F. Parsons, B. W. Ninham, Langmuir 26 (2010) 1816–1823. doi:10.1021/la902533x.

[61] V. A. Parsegian, B. W. Ninham, Journal of Theoretical Biology 38 (1973) 101–109. doi:10.1016/0022-5193(73)90227-0.

[62] V. Esteso, S. Carretero-Palacios, L. G. MacDowell, J. Fiedler, D. F. Parsons, F. Spallek, H. Míguez, C. Persson, S. Y. Buhmann, I. Brevik, M. Boström, Phys. Chem. Chem. Phys. 22 (2020) 11362–11373. URL: http://dx.doi.org/10.1039/C9CP06836H. doi:10.1039/C9CP06836H.

[63] R. R. Dagastine, D. C. Prieve, L. R. White, Journal of Colloid and Interface Science 231 (2000) 351–358. doi:10.1006/jcis.2000.7164.

[64] D. R. Corson, P. Lorrain, Introduction to Electromagnetic Fields and Waves, San Francisco: WH Freeman, 1962.

[65] R. R. Pethig, Dielectrophoresis: Theory, Methodology and Biological Applications, John Wiley & Sons, 2017.

[66] T. Masuda, Y. Matsuki, T. Shimoda, Journal of Colloid and Interface Science 340 (2009) 298–305. doi:10.1016/j.jcis.2009.08.028.

[67] A. Grabbe, Langmuir 9 (1993) 797–801. doi:10.1021/la00027a032.

[68] L. Bergstrom, A. Meurk, H. Arwin, D. J. Rowcliffe, Journal of the American Ceramic Society 79 (1996) 339–348. doi:10.1111/j.1151-2916.1996.tb08126.x.

[69] V. A. Parsegian, G. H. Weiss, Journal of Colloid and Interface Science 81 (1981) 285–289. doi:10.1016/0021-9797(81)90325-8.

[70] F. W. Tavares, D. Bratko, H. W. Blanch, J. M. Prausnitz, The Journal of Physical Chemistry B 108 (2004) 9228–9235. doi:10.1021/jp037809t.

[71] J. Fiedler, M. Boström, C. Persson, I. Brevik, R. Corkery, S. Y. Buhmann, D. F. Parsons, The Journal of Physical Chemistry B 124 (2020) 3103–3113. URL: https://doi.org/10.1021/acs.jpcb.0c00410. doi:10.1021/acs.jpcb.0c00410. arXiv:https://doi.org/10.1021/acs.jpcb.0c00410, pMID: 32208624.

[72] D. F. Parsons, B. W. Ninham, Colloids and Surfaces A: Physicochemical and Engineering Aspects 383 (2011) 2–9. doi:10.1016/j.colsurfa.2010.12.025.

[73] J. B. Hasted, D. M. Ritson, C. H. Collie, The Journal of Chemical Physics 16 (1948) 1–21. doi:10.1063/1.1746645.

[74] J. G. Lessard, M. Fragata, The Journal of Physical Chemistry 90 (1986) 811–817. doi:10.1021/j100277a022.

[75] F. Bellemare, M. Fragata, Journal of Colloid and Interface Science 77 (1980) 243–251. doi:10.1016/0021-9797(80)90437-3.

[76] M. S. Fernandez, P. Fromherz, The Journal of Physical Chemistry 81 (1977) 1755–1761. doi:10.1021/j100533a009.

[77] J. K. Thomas, Chemical Reviews 80 (1980) 283–299. doi:10.1021/cr60326a001.

[78] K. Iwamoto, J. Sunamoto, Bulletin of the Chemical Society of Japan 54 (1981) 399–403. doi:10.1246/bcsj.54.399.

[79] D. R. Laver, J. R. Smith, H. G. L. Coster, Biochimica et Biophysica Acta (BBA) - Biomembranes 772 (1984) 1–9. doi:10.1016/0005-2736(84)90511-X.

[80] S. Kaneshina, H. Kamaya, I. Ueda, Biochimica et Biophysica Acta (BBA) - Biomembranes 777 (1984) 75–83. doi:10.1016/0005-2736(84)90498-X.

[81] P. G. de Gennes, Macromolecules 13 (1980) 1069–1075. doi:10.1021/ma60077a009.

[82] P. de Gennes, F. Brochard-Wyart, D. Quere, Capillarity and Wetting Phenomena: Drops, Bubbles, Pearls, Waves, Springer New York, 2003. URL: https://books.google.de/books?id=MxLQk8vms-kC.

[83] M. Murat, G. S. Grest, Macromolecules 22 (1989) 4054–4059. doi:10.1021/ma00200a041.

[84] J. Eden, P. R. C. Gascoyne, R. Pethig, Journal of the Chemical Society, Faraday Transactions 1: Physical Chemistry in Condensed Phases 76 (1980) 426–434. doi:10.1039/F19807600426.

[85] T. Inagaki, R. N. Hamm, E. T. Arakawa, R. D. Birkhoff, Biopolymers 14 (1975) 839–847. doi:10.1002/bip.1975.360140412.

[86] C. M. Roth, B. L. Neal, A. M. Lenhoff, Biophysical Journal 70 (1996) 977–987. doi:10.1016/S0006-3495(96)79641-8.

[87] W. Fenzl, Zeitschrift für Physik B Condensed Matter 97 (1995) 333–336. doi:10.1007/BF01307484.

[88] E. Evans, M. Metcalfe, Biophysical Journal 46 (1984) 423–426. doi:10.1016/S0006-3495(84)84039-4.

[89] T. J. Su, Lu, R. K. Thomas, Z. F. Cui, J. Penfold, The Journal of Physical Chemistry B 102 (1998) 8100–8108. doi:10.1021/jp981239t.

[90] D. Bendedouch, S. H. Chen, The Journal of Physical Chemistry 87 (1983) 1473–1477. doi:10.1021/j100232a003.

[91] O. Svensson, T. Arnebrant, Journal of Colloid and Interface Science 344 (2010) 44–47. doi:10.1016/j.jcis.2009.12.042.

[92] W. R. Bowen, N. Hilal, R. W. Lovitt, C. J. Wright, J. Colloid Interface Sci. 197 (1998) 348–352. doi:10.1006/jcis.1997.5247.

[93] J. N. Munday, F. Capasso, V. A. Parsegian, Nature 457 (2009) 170–173. URL: https://doi.org/10.1038/nature07610.

[94] P. J. van Zwol, G. Palasantzas, Phys. Rev. A 81 (2010) 062502. URL: https://link.aps.org/doi/10.1103/PhysRevA.81.062502. doi:10.1103/PhysRevA.81.062502.

[95] M. Boström, B. W. Ninham, I. Brevik, C. Persson, D. F. Parsons, B. E. Sernelius, Applied Physics Letters 100 (2012) 253104. URL: https://doi.org/10.1063/1.4729822. doi:10.1063/1.4729822. arXiv:https://doi.org/10.1063/1.4729822.

[96] M. Boström, M. Dou, O. I. Malyi, P. Parashar, D. F. Parsons, I. Brevik, C. Persson, Phys. Rev. B 97 (2018) 125421. URL: https://link.aps.org/doi/10.1103/PhysRevB.97.125421. doi:10.1103/PhysRevB.97.125421.

[97] J. D. Ferry, J. L. Oncley, Journal of the American Chemical Society 63 (1941) 272–278. doi:10.1021/ja01846a067.

[98] S. Takashima, Biochimica et Biophysica Acta (BBA) - Specialized Section on Biophysical Subjects 79 (1964) 531–538. doi:10.1016/0926-6577(64)90218-9.

[99] P. Moser, P. Squire, C. O'Konski, The Journal of Physical Chemistry 70 (1966) 744–756.

[100] M.-J. Dejardin, A. Hemmerle, A. Sadoun, Y. Hamon, P.-H. Puech, K. Sengupta, L. Limozin, Nano Letters 18 (2018) 6544–6550. URL: https://doi.org/10.1021/acs.nanolett.8b03134. doi:10.1021/acs.nanolett.8b03134. arXiv:https://doi.org/10.1021/acs.nanolett.8b03134, pMID: 30179011.

Graphical Abstract

On the Control of Dispersion Interactions Between Biological Membranes and Protein Coated Biointerfaces

Robert Blackwell,Arnaud Hemmerle,Andreas Baer,Matthias Späth,Wolfgang Peukert,Drew Parsons,Kheya Sengupta,Ana-Sunčana Smith

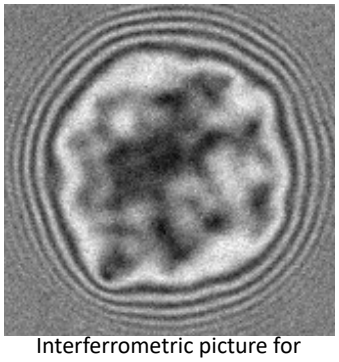
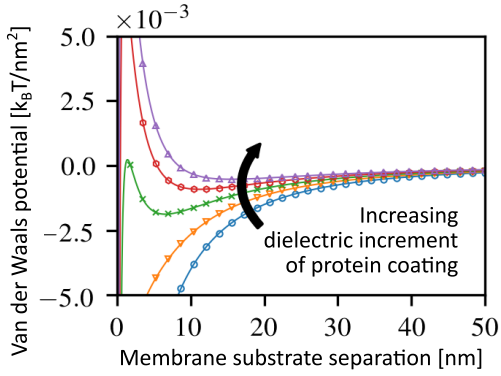
Interferrometric picture for separation measurements